RRAM Devices with Plasma Treated HfO_2 with Ru as Top Electrode for In-Memory Computing Hardware

ECS Transactions, 104 (3) 35-44 (2021)
10.1149/10403.0035ecst ©The Electrochemical Society

RRAM Devices with Plasma Treated HfO_2 with Ru as Top Electrode for In-Memory Computing Hardware

Y.D. Patel,[1] D. Misra,[1] D.H. Triyoso,[2] K. Tapily,[2] R.D. Clark,[2] S. Consiglio,[2] G. Pattanaik[2], C. Cole[2], A. Raley[2], C.S. Wajda,[2] and G.J. Leusink[2]

[1]ECE Dept, NJIT, Newark, NJ 07102, USA
[2]TEL Technology Center, America, LLC, Albany, NY 12203, USA

This work investigates the role of extra oxygen vacancies, introduced by a hydrogen plasma at midpoint of deposition of a 6 nm thick HfO_2 to reduce the switching power consumption in a RRAM device. Initially TiN, which is a commonly used metal in CMOS technology, was used as the top electrode for treated HfO_2. Subsequently Ru and TaN as top electrodes were explored to enhance the switching behavior and power consumption. A range of compliance currents from 1 nA to 1 μA were used to evaluate the switching characteristics. The role of both TaN and Ru as bottom metal was also evaluated. With Ru as top metal the device switched at a compliance current of 1 nA and higher. Whereas when Ru was used as bottom electrode, devices were unable to switch below a compliance current of 50 μA. For TaN as top metal electrode, devices switched at and above 1 μA CC whereas with TaN as bottom metal the initial switching was at CC of 2 μA. It was observed that use of Ru as a top metal significantly reduced the switching energy of the plasma treated HfO_2 RRAM device but was ineffective when used as a bottom metal.

Introduction

Recently, deep neural networks (DNNs) have been extensively used for in-memory computing for various machine learning applications. Many of the proposed hardware approaches have the limitations with respect to power, area, and training time. Therefore, the in-memory computing and artificial intelligence hardware requires that innovative physical properties of non-volatile memories such as two-terminal resistive random access memory (RRAM) be explored. Furthermore, the RRAM devices are an ideal choice for implementing electrical synapses due to their small size, enabling them to be densely packed in crossbar arrays. RRAM technology has proved itself in many aspects of semiconductor technologies, like high-speed switching, high storage density, enhanced scalability, and retaining multiple bits in a single device. Although such characteristics such as endurance, retention, power reduction, and controllability of switching characteristics are being investigated further (1) to utilize it for AI hardware and neuromorphic computing hardware, RRAM technologies provide unique advantages of storing the synaptic weights. The typical RRAM's structure consists of an insulator sandwich between two metals, in the shape of a metal-insulator-metal capacitor. The resistance of the insulator that serves as the switching layer is modified when an electric field is applied to the top and bottom metal electrodes because of formation and rupture of a conducting filament. Depending on the structural composition of the switching layer of the RRAM and the choice of top metal and the bottom

electrode, the switching characteristics (setting and resetting process) and switching power requirement differ. In addition, the oxygen vacancy distribution and migration effects are responsible for the modification of the synaptic weights.

HfO_2-based dielectrics with controlled distribution of defects or oxygen vacancies can potentially enable low power switching and multi-resistance (conductance) levels. However, detailed studies of the power consumption, repeatability, non-ideal characteristics such as finite conductance resolution, spatial conductance variability during programming and read, retention during multi-level operation have not been undertaken. Besides, lack of enough oxygen vacancies in stoichiometric HfO_2 limits the low power operation. Therefore, HfO_x (with $x < 2$) has been studied for many RRAM devices (2). A uniform distribution of defects in HfO_2 may help in switching but may not help in reducing the switching power. During reset process the reconstruction of the ruptured filament near the top electrode typically takes place. We have recently reported that asymmetric oxygen vacancy distribution with a higher concentration close to top electrode tends to reduce the switching power (3). The distribution of these defects throughout the bulk of HfO_2 is, therefore, not well-understood.

Additionally, the electrode metals play a significant role since the switching operation is mainly dominated by a thin section closer to the electrodes (4). Physical properties such as metal work function and metal/dielectric barrier heights are highly responsible for switching mechanism. The role of top electrode is found to be superior as compared to bottom electrode for oxygen migration. Furthermore, the oxygen concentration at the dielectric and metal interface can modulate the work function of the top metal. It is because an oxygen deficient interface can lower the work function whereas excess oxygen can increase of work function (5). The metal/dielectric barrier height also changes with the interface oxygen concentration. Deficiency in oxygen atoms can lead to barrier lowering (6). Therefore, it is critical to carefully select the top electrode metal to reduce the switching power and overall power consumption.

In this work, the role of extra oxygen vacancies, introduced by hydrogen plasma for a 6 nm thick HfO_2 during deposition to reduce the power consumption, is investigated. The purpose is to evaluate the controlled distribution of additional oxygen vacancies/defects by modifying the process conditions such as insertion of plasma treatment at the middle of the HfO_2 deposition process. It is believed that this process step may create an oxygen vacancy rich HfO_2 near the top electrode that will reduce the switching power and enhance the switching behavior. Initially TiN, which is a commonly used metal in CMOS technology and enhances the oxygen vacancy creation (7), was used as the top electrode for treated HfO_2 using a Si/PVD Ti/PVD TiN/HfO_2/PVD TiN structure. A range of compliance currents (ICC) from 1 nA to 500 nA were used to evaluate the switching characteristics. Subsequently, TaN and Ru electrodes were explored to further investigate the impact of top and bottom metals on the switching behavior and power consumption.

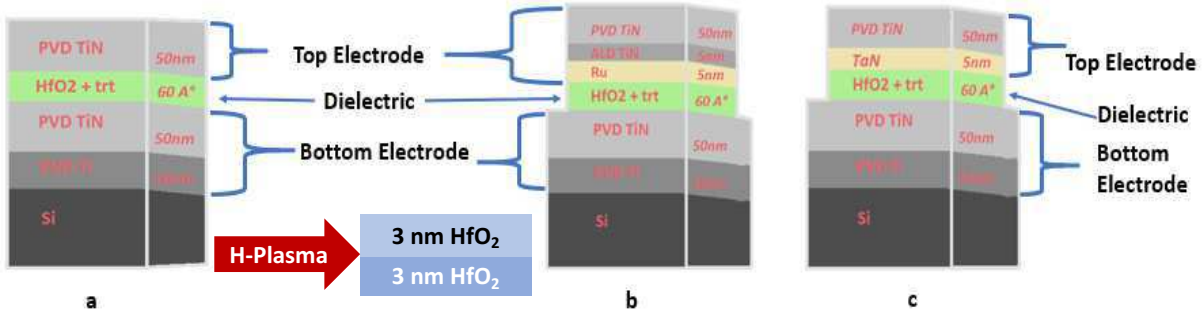

Figure 1. RRAM devices were fabricated with common bottom electrodes of 10 nm PVD Ti followed by 50 nm PVD TiN and with three different top metal electrodes: (a) 50 nm TiN, (b) 5 nm Ru followed by 5 nm of ALD TiN and 50 nm of PVD TiN and (c) 5 nm TaN followed by 50 nm of PVD TiN.

Experimental

The MIM structures were fabricated on 300 mm silicon wafers starting with 10 nm physical vapor deposition (PVD) Ti followed by 50 nm PVD TiN. A 6-nm thick ALD HfO_2 was then deposited in an ALD reactor. Details of the fabrication process are explained in detail elsewhere (8, 9). The samples were subjected to hydrogen plasma (H-Plasma) at the middle of the deposition process (after 3-nm of HfO_2 deposition) in a clustered microwave plasma chamber (10) to incorporate excess oxygen vacancies. After HfO_2 deposition three different top metal electrodes were deposited as shown in Fig. 1 with 50 nm of PVD TiN (Fig. 1(a), herein denoted as TiN devices), 5 nm ALD Ru followed by 5 nm of ALD TiN and 50 nm of PVD TiN (Fig. 1(b), herein denoted as Ru devices) and 5 nm ALD TaN followed by 50 nm of PVD TiN (Fig. 1(c), herein denoted as TaN devices). Fig. 1 inset shows the H-Plasma treatment at the middle of deposition. The top electrodes were patterned to for the MIM capacitors. In some cases, the dielectric layers were etched along with the top electrodes to expose the bottom electrodes.

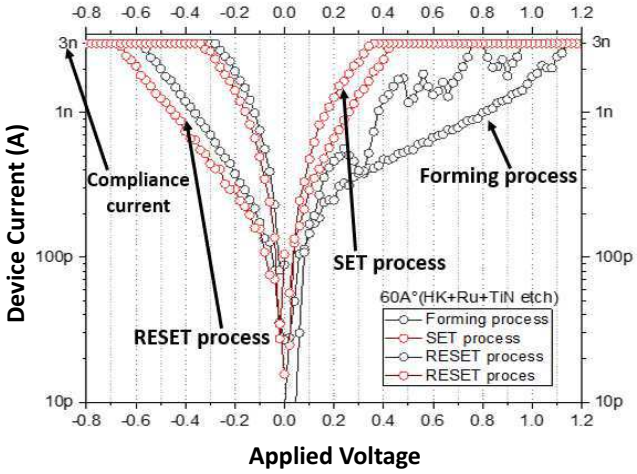

Figure 2. A typical bipolar switching characteristic of an RRAM cell with forming, set, and reset steps with a compliance current of 3 nA.

Electrical characterization was performed using a Keysight B1500 semiconductor device parameter analyzer on 100 μm^2 x 100 μm^2 MIM capacitors. A typical bipolar switching

characteristic of a RRAM cell is shown in the Fig. 2 with forming, set, and reset steps. Initially, during the forming process the current increases and reaches the 3 nA, the compliance current set for this device by the parameter analyzer, to form the filament. Once the filament is formed, current increases (black circles) and the device enters the low resistance state (LRS). During the reset process, current decreases as the filament ruptures and the device enters the high resistance state (HRS). The subsequent set process does not require forming the entire filament but reconstructing the ruptured portion of the filament at a lower voltage (red circles) compared to initial forming voltage. In some devices, with the same metal electrodes, no forming voltage was observed for the set process. For the power requirement analysis, the switching characteristics was initiated with extremely low compliance current of 1 nA and gradually increased further till the devices start switching. Compliance currents were increased carefully to avoid any irreversible device breakdown.

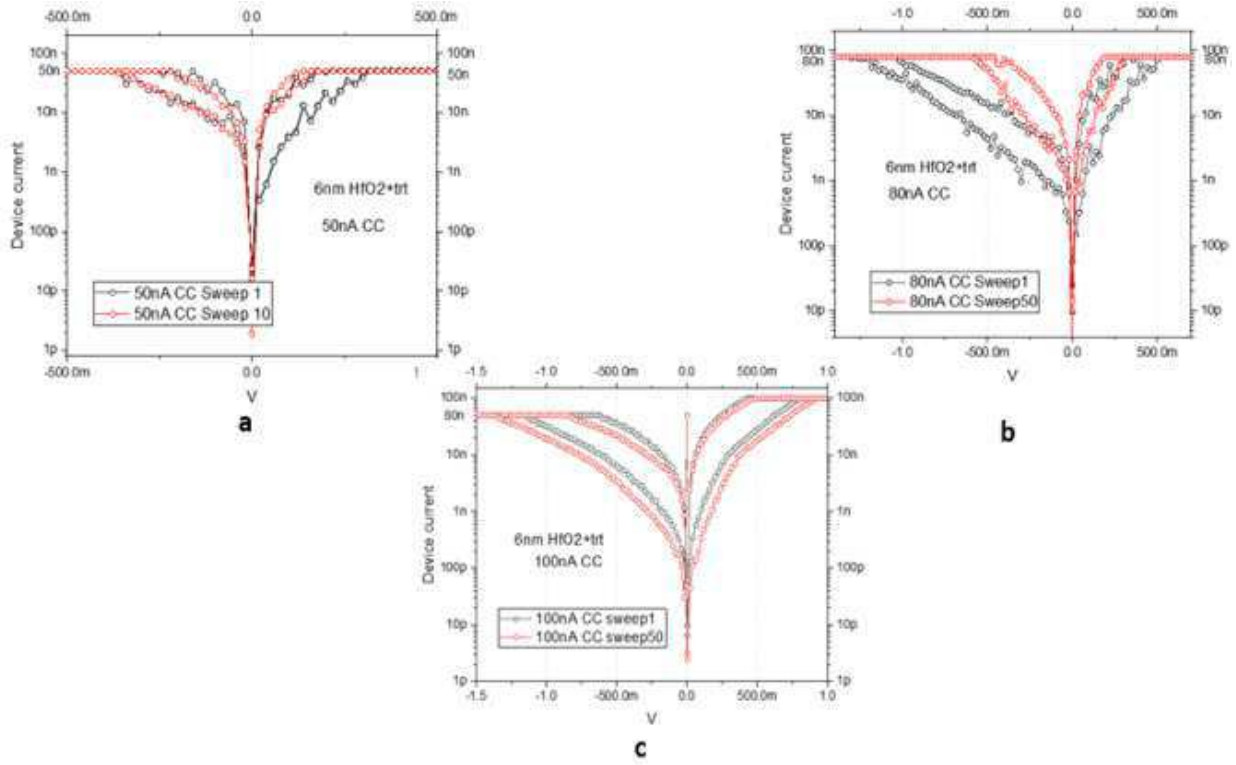

Figure 3. I-V characteristics of TiN devices showing at least two different sweeps (1st and 50th sweep) with different compliance currents, (a) 50 nA, (b) 80 nA and (c) 100 nA.

Results and Discussions

Fig. 3(a), Fig. 3(b) and Fig. 3(c) show the bipolar current-voltage (I-V) characteristics of TiN devices (Fig. 1(a)) with different compliance currents, 50 nA, 80 nA, and 100 nA respectively. Forming process was carried out by gradually increasing the compliance current from 3 nA up to 100 nA and most of the devices first switched at 50 nA and were tested for sustainability for hundreds of cycles. The first sweep typically initiated the forming process. The average minimum switching power (11) for set or reset ($P_{Set,\ Reset} = V_{Set,\ Reset} \times I_{CC}$) for TiN devices is approximately 15 nW. This is a significant reduction in switching power compared to other reported TiN devices

(6, 12). The hydrogen plasma treatment may be the reason for the reduced the power. Bhuyian *et al* (13) reported that plasma treatment of the exposed layer is densified, and the subsequent layer has a higher density of defects. One possible explanation for this observation is that the defects created during the plasma treatment were passivated during the top layer deposition as oxygen from the top layer reduced the oxygen vacancy related defects in the plasma exposed layer. These defects, therefore, could migrate towards the top electrode increasing the oxygen vacancy concentration at the top of bulk dielectric. Consiglio *et al* (14) observed similar behavior when their forming voltage decreased when a post plasma exposure HfO_2 cap layer was deposited. One possible mechanism for this observation is that the oxygen atoms from the cap layer diffused into the bottom layer leaving higher oxygen vacancy concentration towards the top of the dialectic, near the top electrode (14). When a thinner cap layer is deposited after plasma treatment, it is not able to re-oxidize the defects and the distribution of oxygen vacancy related defects becomes uniform throughout the dielectric thickness. That leads to a higher forming voltage. Whereas when a thicker cap layer is used, the re-oxidation followed by oxygen vacancy migration toward the top reduces the forming voltage (14). In our case, we believe that the plasma treatment at midpoint of HfO_2 deposition increases the oxygen vacancy related defects close to the top electrode that significantly decreased the switching power for filament formation.

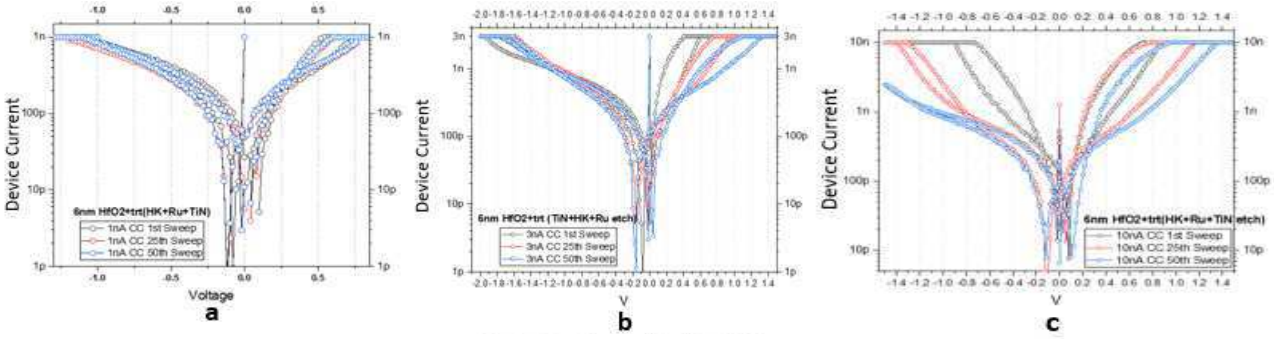

Fig. 4. 2 I-V characteristics of the devices with Ru as top electrode are shown. (a) Three (1st, 25th, and 50th) set-reset sweeps are shown with CC of 1nA, (b) Three (1st, 25th, and 50th) set-reset sweeps are shown with CC of 3nA (c) Three (1st, 25th, and 50th) set-reset sweeps are shown with CC of 10nA.

By varying the top metal, we evaluated the RRAM devices with Ru as the top electrode (Fig. 1(b)). Fig. 4 shows the I-V characteristics of Ru devices with the Si/PVD Ti/PVD TiN/HfO_2/Ru/PVD TiN structure for three different compliance currents, 1 nA (Fig. 4(a)), 3 nA (Fig. 4 (b)), and 10 nA (Fig. 4 (c)). The device switched at a minimum of 1 nA of compliance current showing a very low power of P_{Set} = 0.75 nW and P_{Reset} = 1 nW (Fig. 4(a)). A tighter distribution of SET and RESET cycles of 50 cycles of the switching process was observed. The reduction of the switching power is mostly due to the presence of Ru as top metal in addition to plasma treatment. While the oxygen vacancy or defect distribution due to plasma treatment is high near the top electrode as described above, the metal/HfO_2 interface characteristics plays a significant role in power reduction. While the higher work function determines a stable resistive switching (15), the change in barrier height between and the dielectric dominates the switching power. The work function of Ru/HfO_2 is 4.6 eV (4) which is slightly higher than TiN (4.5 eV). Pantisano *et al* (6) reported that the defects in the dielectric layer rather than metal-induced gap states control the barrier height. Besides, Ru being less reactive than TiN, oxygen deficiency at the

Ru/HfO_2 interface contributes to additional barrier lowering (6). Note that for the case of 3 nA and 10 nA compliance currents, the set and reset voltages increased during the subsequent cycles. Possible redistribution of oxygen ions immediately after the set or reset process due to interaction of oxygen vacancies with top metal is responsible for this behavior. Furthermore, Ru deposition process played a role in power reduction (3).

We then evaluated TaN as the top metal to investigate the switching power requirements. As shown in the Fig. 5, much higher compliance current of 1.3 μA was required for the device to form the conducting filament and be able to switch between LRS and HRS states. Fig. 5(a) shows three cycles with a compliance current of 1.3 μA where the devices were less stable and the reset and set cycles were not well defined. The device performance was maintained for the 50 switching cycles that were used. Higher CC with 1.5uA and 2uA are shown in Fig. 5(b) and Fig. 5(c) respectively. Some devices formed a permanent non-reversible conducting filament after several switching cycles, which shows a reduced stability. TaN has high reactivity toward oxygen, and it oxidizes to TaON because of oxygen scavenging property. The interfacial layer between the TaN and dielectric forms a non-uniform oxide layer which further changes the interface properties and helps in the switching characteristics (16). In our devices the excess oxygen vacancies close to the top electrode was possibly reduced because of TiON formation and increased the minimum switching compliance current.

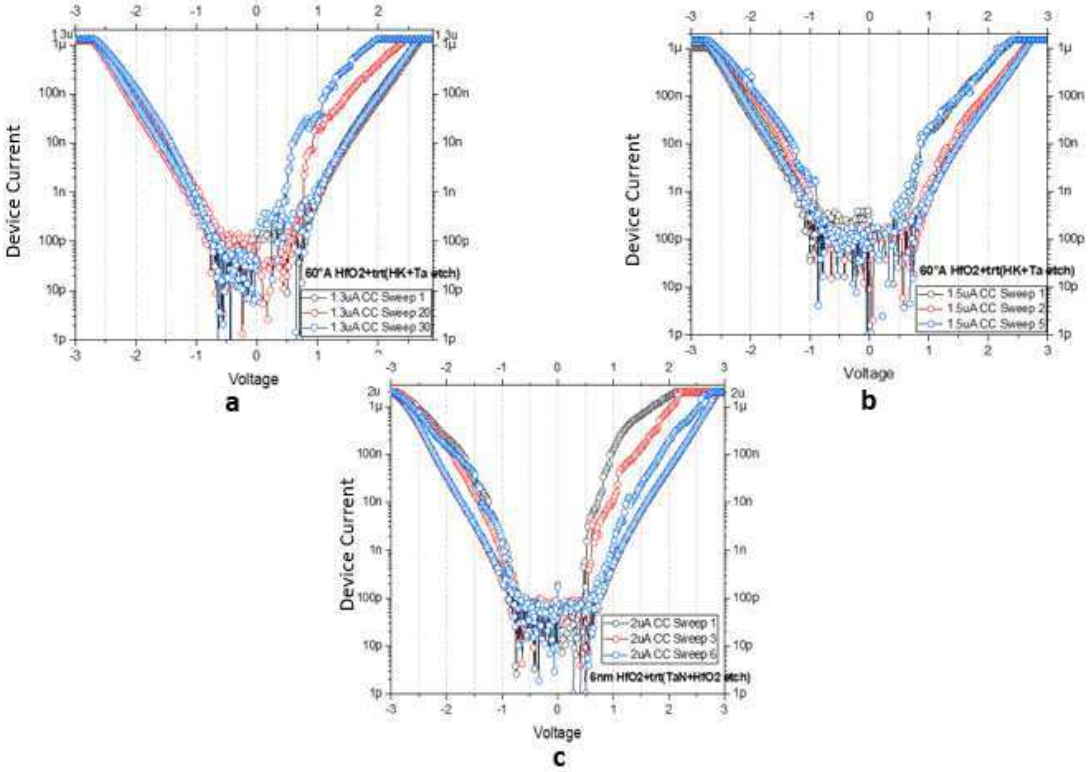

Fig. 5. I-V characteristics of the devices with TaN as top electrode is shown. (a) Three (1st, 20th, and 30th) set-reset sweeps are shown with compliance current of 1.3uA (b) Three (1st, 2nd, and 5th) set-reset sweeps are shown with compliance current of 1.5uA. (c)Three (1st, 3rd, and 6th) set-reset sweeps are shown with compliance current of 2uA.

Assuming the initial oxygen vacancy distribution in the plasma treated HfO_2 layer is identical, the switching characteristics demonstrate a significant variation. The top electrode material is, therefore, responsible for the observed variation. Ru has one electron in its outer most orbit while Ta and Ti has two electrons. Schottky barrier height is changed by top electrode if the oxygen is weakly bonded in the dielectric layer (17). The reduction of the switching power is mostly due to the presence of Ru as a top metal in addition to plasma treatment. It is evident that metal/HfO_2 interface characteristics plays a significant role in power reduction. While higher work function determines a stable resistive switching, the change in barrier height between and the dielectric dominates the switching power. The defects in the dielectric layer rather than metal-induced gap states control the barrier height. Ru being less reactive than TiN and TaN, oxygen deficiency at the Ru/HfO_2 interface contributes to additional barrier lowering. Ru deposition process plays a role in power reduction and interfacial structural differences affect electrical properties during the conducting filament formation. Ru and TaN as bottom electrode increased the minimum compliance current even higher (not shown). The top metal, therefore, is more dominant when the defects on the top part of the HfO_2 is higher than that of the bottom layer.

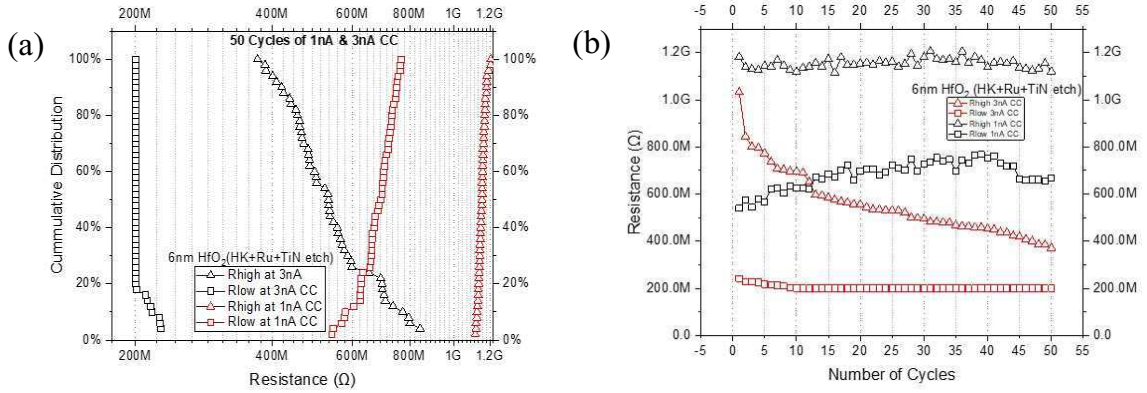

Fig. 6. Cumulative Resistance distribution of the devices with Ru as top electrode is shown. (a) Cumulative distribution of resistance of 50 cycles at 0.6V with 3nA CC and at 0.54V with 1nA CC, (b) Resistance variation across the 50 cycles for both the compliance currents.

Fig. 6 shows the resistance switching behavior with high resistance and low resistance values and HRS and LRS measured at 0.54 V and 0.6 V respectively. Fig. 6(a) shows the cumulative distribution vs resistance plots of the Ru top electrode devices (Fig. 1(b)) for 1 nA and 3 nA compliance currents. R_{high} represents the resistance at HRS, while R_{low} represents the resistance at LRS. Two different compliance currents were used to assess whether the devices are stable for multilevel resistance values. Figure 6(b) shows the resistance variation across the 50 cycles for both the compliance currents. It is known that every switching cycle can introduce resistance drifts due to possible permanent damage. Devices with 1 nA compliance current showed a minimum drift for the entire evaluation cycles whereas devices with 3 nA compliance current showed noticeable drifts. This drift in 3 nA compliance current can be attributed to the degradation due to reduced number of ions in the active region (18).

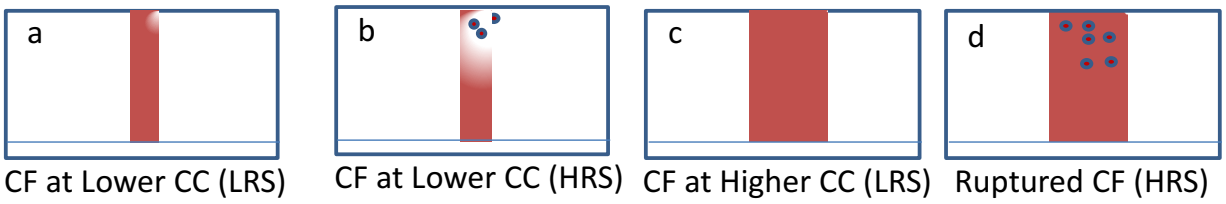

Fig. 7. Conducting Filament formation as a function of compliance current (a) at lower compliance current (LRS), (b) Ruptured CF at lower compliance current (HRS), (c) at a higher compliance current (LRS), and (c) ruptured CF at higher compliance current (HRS).

In addition, there was a stark difference in resistance values. At low compliance current, the conducting filament is thin or only a few conducting paths were created. Whereas at higher compliance currents, a thick conducting filament or many conducting paths were created. The schematic in Fig. 7 shows that lower compliance current leads to higher R_{low} as compared to R_{low} for higher compliance current. The reverse is true for R_{high} because of the spread of the ruptured conducting filament. This characteristic demonstrates that by adjusting the resistance according to the requirement can implement multilevel capability. It can be, therefore, assumed that switching at lower current can have better resistance distribution over large number of cycles.

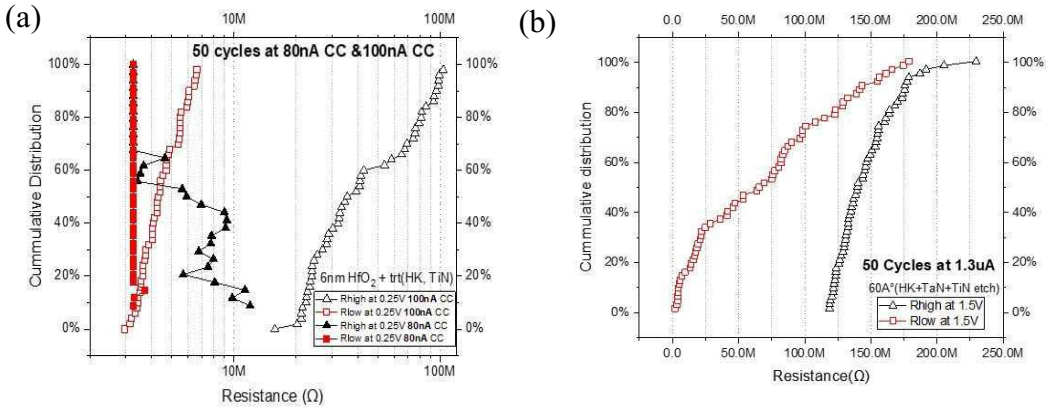

Fig. 8. (a) Cumulative Resistance distribution of the devices with TiN as top electrode for 50 cycles at 0.25V with 100nA and 80nA of compliance current; (b) Cumulative Resistance distribution of the devices with TaN as top electrode is shown. Resistance distribution of 50 cycles at 1.25V with 1.3uA compliance current.

The resistance distribution for TiN as a top electrode metal is quite different because of its reactivity with oxygen ions and scavenging oxygen from the switching dielectric. Fig. 8(a) shows the cumulative resistance distribution of TiN device for 50 SET-RESET cycles at 80 nA and 100 nA of CC measured 0.25V. The resistance variation across the cycles shows a decrease in resistance value as cycle number is increased except for R_{low} at 80 nA CC. As mentioned earlier the TiN RRAM devices showed the resistance values are much smaller than Ru devices. It is because after the metal deposition excess oxygen ions were scavenged to the TiN/HfO_2 interface. Fig. 8(b) shows the cumulative resistance distribution of TaN device for 50 SET-RESET cycles at 1.3 uA of compliance current measured at 1.5V. The resistance distribution of TaN has a spread for both HRS and LRS, showing that set voltage is not very controlled. As mentioned earlier, the SET voltage increases as the cycles proceed. TaN has similar oxygen scavenging properties as

TiN, but different work function and Schottky barrier that can be a possible explanation for less endurance and less controllability of CF.

Conclusions

We have evaluated the HfO_2 as the switching layer for a RRAM device that can be used for in-memory computing hardware. Additional oxygen vacancies were introduced by a hydrogen plasma treatment at midpoint of deposition of a 6 nm thick HfO_2 to reduce the switching power of the device. We have also implemented three different metals, TiN, Ru, and TaN, as the top electrode and studied their impact in power reduction. We believe that the hydrogen plasma treatment at midpoint may enhance the oxygen vacancy concentration near to the top electrode resulting in a graded distribution. The graded distribution may in turn result in the reduction of switching power requirement. The use of Ru as the top electrode reduced the set and reset power to 750 pW and 1 nW respectively for switching. This could be attributed to the Ru barrier height and reaction with oxygen ions. As a top metal, TiN has significant decrease in switching power compared to reported values but TaN did not show much reduction in power. The resistance distribution seems to be better at low compliance currents.

Acknowledgement

This work was partially supported by a National Science Foundation grant (#EECS-1710009).

References

1. B. Yan, B. Li, X. Qiao, C-X. Xue, M.-F. Chang, Y. Chen, and H. Li, *Adv. Intell. Syst.*, 1, 1900068 (2019).
2. W. Chen, W. Lu, B. Long, Y. Li, D. Gilmer, G. Bersuker, S. Bhunia, and R. Jha, *Semiconductor Science and Technology* **30**, 075002 (2015).
3. D. Misra, P. Zhao, D. H. Triyoso, V. Kaushik, K. Tapily, R. D. Clark, S. Consiglio,2, T. Hakamata, C. S. Wajda, and G. J. Leusink, *ECS J. Solid State Sci. Technol*. 9, 05300, (2020).
4. K.M. Kim, B. J. Choi, and C. S. Hwang, *Appl. Phys. Lett.*, 90, 242906 (2007).
5. H.Y. Lee, P.S. Chen, T.Y. Wu, C.C. Wang, P.J. Tzeng, C.H. Lin, F. Chen, M-J. Tsai, and C, Lien, *Appl. Phys. Lett.,* 92, 142911 (2008).
6. L. Pantisano, V.V. Afanas'ev, S. Cimino, C. Adelmann, L. Goux, Y.Y. Chen, J.A. Kittl, D. Wouters and M. Jurczak, *Microelectronic Engineering*, 88, 1251, (2011).
7. Y. Fang, Z. Yu, Z. Wang, T. Zhang, Y. Yang, Y. Cai and R. Huang, *IEEE Electron Device Lett*., 39(6), 819, (2018).
8. R. D. Clark, S. Consiglio, C. S. Wajda, G. J. Leusink, T. Sugawara, H. Nakabayashi, H. Jagannathan, L. F. Edge, P. Jamison, V. K. Paruchuri, R. Iijima, M. Takayanagi, B. P. Linder, J. Bruley, M. Copel, and V. Narayanan, *ECS Trans.*, 16(4), 291 (2008).
9. K. Tapily, S. Consiglio, R. D. Clark, R. Vasi´c, E. Bersch, J. Jordan-Sweet, I. Wells, G. J. Leusink, and A. C. Diebold, *ECS Trans.*, 45(3), 411 (2012).
10. T. Sugawara, S. Matsuyama, M. Sasaki, T. Nakanishi, S. Murakawa, J. Katsuki, S. Ozaki, Y. Tada, T. Ohta, and N. Yamamoto, *Jpn. J. Appl. Phys*., 44, 1232 (2005).
11. Y-J. Huang, T-H. Shen, L-H. Lee, C-Y. Wen and S-C. Lee, *AIP Advances***,** 6, 065022 (2016).

12. Y.Y. Chen, L. Goux, L. Pantisano, J. Swerts, C. Adelmann, S. Mertens, V.V. Afanasiev, X.P. Wang, B. Govoreanu, R. Degraeve, S. Kubicek, V. Paraschiv, B. Verbrugge, N. Jossart, L. Altimime, M. Jurczak, J. Kittl, G. Groeseneken and D.J. Wouters, *Microelectronc Engineering*, 112, 92, (2013).
13. M. N. Bhuiyan, D. Misra, K. Tapily, R. D. Clark, S. Consiglio, C. S. Wajda, G. Nakamura, and G. J. Leusink, *ECS J. Solid State Sci. and Technol.*, 3(5), N83, (2014).
14. S. Consiglio, H. Higuchi, T. Ando, P. Jamison, S. C. Seo, D. Kong, Y. Kim, K. Tapily, R. D. Clark, M. Hopstaken, E. Cartier, T. Tsunomura, C. S. Wajda, R. Soave, V. Narayanan, G. J. Leusink, *ECS Trans.*, 102(2), 19 (2021).
15. Z. Wei, Y. Kanzawa, K. Arita, Y. Katoh, K. Kawai, S. Muraoka, S. Mitani, S. Fujii, K. Katayama, M. Iijima, T. Mikawa, T. Ninomiya, R. Miyanaga, Y. Kawashima, K. Tsuji, A. Himeno, T. Okada, R. Azuma, K. Shimakawa, H. Sugaya, T. Takagi, R. Yasuhara, K. Horiba, H. Kumigashira and M. Oshima, *IEDM Technical Digest*, 293, (2008).
16. M. Ismail, E. Ahmed, A.M. Rana, I. Talib, T. Khan, K. Iqbal and M.Y. Nadeem, *Thin Solid Films*, 583, 95, (2015).
17. S. Slesazeck and T, Mikolajick, *Nanotechnology*, 30(35), 352003, 2019.
18. F. Zahoor, T. Zulkifli and F.A. Khanday, *Nanoscale Research Letter*, 15, 90, (2020).